nature chemical biology

SUPPLEMENTARY INFORMATION

https://doi.org/10.1038/s41589-019-0369-4

In the format provided by the authors and unedited.

A lipid site shapes the agonist response of a pentameric ligand-gated ion channel

Camille M. Hénault[1], Cedric Govaerts[2], Radovan Spurny[3], Marijke Brams[3], Argel Estrada-Mondragon[4], Joseph Lynch[4], Daniel Bertrand[5], Els Pardon[6,7], Genevieve L. Evans[3], Kristen Woods[8,9], Benjamin W. Elberson[10], Luis G. Cuello[10], Grace Brannigan[8,9], Hugues Nury[11], Jan Steyaert[6,7], John E. Baenziger[1]* and Chris Ulens[3]*

[1]Department of Biochemistry, Microbiology and Immunology, University of Ottawa, Ottawa, Ontario, Canada. [2]Laboratory for the Structure and Function of Biological Membranes, Center for Structural Biology and Bioinformatics, Université libre de Bruxelles, Brussels, Belgium. [3]Laboratory of Structural Neurobiology, Department of Cellular and Molecular Medicine, KU Leuven, Leuven, Belgium. [4]Queensland Brain Institute, University of Queensland, Brisbane, Queensland, Australia. [5]HiQscreen, Vésenaz, Geneva, Switzerland. [6]Structural Biology Brussels, Vrije Universiteit Brussel, Brussels, Belgium. [7]VIB-VUB Center for Structural Biology, VIB, Brussels, Belgium. [8]Center for Computational and Integrative Biology, Rutgers University–Camden, Camden, NJ, USA. [9]Department of Physics, Rutgers University–Camden, Camden, NJ, USA. [10]Department of Cell Physiology and Molecular Biophysics, Center for Membrane Protein Research, TTUHSC, Lubbock, TX, USA. [11]University Grenoble Alpes, CNRS, IBS, Grenoble, France. *e-mail: john.baenziger@uottawa.ca; chris.ulens@kuleuven.be

	ELIC 7'C + Nb72	ELIC Δ8 + Nb72	ELIC F16'S (alternate M4)
Data collection			
Space group	$P2_1$	$P2_1$	$P2_1$
Cell dimensions			
a, *b*, *c* (Å)	96.25, 156.28, 102.50	95.68, 155.09, 101.62	105.80, 264.70, 111.19
β (°)	102.88	103.08	108.80
Resolution (Å)	48.84 - 2.50 (2.64 - 2.50)	49.49 - 2.78 (2.85 - 2.78)	48.90 - 3.45 (3.52 - 3.45)
R_{merge}	6.7 (94.8)	9.8 (144.2)	13.3 (136.5)
$I / \sigma I$	14.8 (1.3)	6.6 (0.6)	6.7 (1.0)
Completeness (%)	99.9 (99.9)	99.3 (92.7)	99.8 (99.9)
Redundancy	3.5 (3.4)	3.3 (2.9)	3.9 (4.1)
Refinement			
Resolution (Å)	47.59-2.50	49.49 - 2.78	19.99-3.45
No. reflections	101739	71790	75338
R_{work} / R_{free}	20.42 / 24.51	22.53 / 23.25	22.78 / 26.55
No. atoms			
Protein	16616	16080	24972
Ligand/ion	302		240
Water	308		
B-factors			
Protein	59.14	101.39	112.38
Ligand/ion	84.16		150.71
Water	51.95		
R.m.s. deviations			
Bond lengths (Å)	0.002	0.008	0.004
Bond angles (°)	0.506	1.03	0.741

Supplementary Table 1 | X-ray diffraction data and structure refinement statistics.

Beam wavelengths, resolution cutoff criteria, MolProbity scores and Ramachandran statistics are reported in the Methods section.

* Highest-resolution shell is shown in parentheses.

* All data sets were obtained from single crystals.

Bilayer type	Time constant of desensitization, τ (sec)	I_{max} (nA)
asolectin	12.93 ± 5.16 (n=26)	1.28 ± 0.61 (n=26)
asolectin + cholesterol	38.82 ± 6.46 (n=6)	0.75 ± 0.05 (n=6)
PC/PE/PG	ND (n=16)	1.94 ± 0.52 (n=16)
PC/PG	ND (n=10)	1.00 ± 0.56 (n=10)

Supplementary Table 2 | Data statistics for electrophysiological recordings of ELIC reconstituted in lipid vesicles.

Time constants of activation and peak current amplitudes for the lipid vesicle recordings shown in Figure 2d. Values are for the agonist response to 30 mM GABA in vesicles of different lipid composition. Data are reported as the mean ± SEM from 6 to 26 independent experiments. PC (1-palmitoyl-2-oleoyl-glycero-3-phosphocholine), PG (1-palmitoyl-2-oleoyl-sn-glycero-3-phospho-(1'-rac-glycerol)) and PE (1-palmitoyl-2-oleoyl-sn-glycero-3-phosphoethanolamine).

	Slope ($s^{-1}M^{-1}$)	EC_{50} cysteamine (mM)
I281A	3.07 ± 0.80 (n=6)	0.26 ± 0.02
A217G+W220A	2.39 ± 1.08 (n=3)	0.69 ± 0.08
W220A	1.28 ± 0.61 (n=9)	0.76 ± 0.18
W224R	0.98 ± 1.45 (n=7)	0.42 ± 0.08
F274A	0.82 ± 0.76 (n=8)	0.96 ± 0.12
A217G	< 0.01 (n=8)	0.91 ± 0.17
F282A	< 0.01 (n=7)	0.045 ± 0.02

Supplementary Table 3 | Data statistics for electrophysiological recordings of ELIC mutants in the lipid binding site.

Slope values and EC_{50}-values for mutants in the lipid binding site. Traces are shown in Supplementary Figure 7. The slope values reported in this table are obtained from the reciprocal time constant of activation ($1/\tau$) plotted as a log function of agonist concentration (the procedure is shown in Supplementary Figure 8). Data are reported as the mean ± SEM from 3 to 9 independent experiments.

	Slope ($s^{-1}M^{-1}$)
α7 nAChR	32.43 ± 2.97 (n=8)
ELIC Δ8	26.84 ± 1.43 (n=5)
ELIC ΔM4	23.48 ± 1.23 (n=4)
ELIC P305A	18.21 ± 0.37 (n=5)
ELIC P305A+L309P	14.30 ± 0.94 (n=6)
ELIC P305A+I297P	4.83 ± 0.33 (n=4)
ELIC P305A+R301P	2.34 ± 0.12 (n=6)
wild type ELIC	< 0.01

Supplementary Table 4 | Quantitative analysis of ELIC desensitization kinetics
The slope values reported in this table are obtained from the reciprocal time constant of activation ($1/\tau$) plotted as a log function of agonist concentration (Supplementary Figure 8). Values are presented as the mean ± SEM from 4 to 8 independent experiments.

ELIC mutants	ΔI Cysteamine EC_{50} (mM)	I_{max} (μA)	ΔF Cysteamine EC_{50} (mM)	ΔF_{max} (%)	n
WT	0.21 ± 0.03	5.1 ± 0.2	-	0.1 ± 0.1	7
G319C	0.32 ± 0.01	6.4 ± 0.1	0.13 ± 0.01	3.5 ± 0.1	5
I320C	0.40 ± 0.04	6.3 ± 0.2	0.27 ± 0.02	4.4 ± 0.2	7
T321C	0.23 ± 0.01	9.4 ± 0.3	0.19 ± 0.02	5.3 ± 0.1	7
G322C	0.31 ± 0.01	11.4 ± 0.2	0.18 ± 0.02	6.7 ± 0.1	7

ELIC (ANAP)	ΔI Cysteamine EC_{50} (mM)	I_{max} (μA)			n
WT	0.23 ± 0.03	1.9 ± 0.3			7
F304X	0.24 ± 0.05	0.7 ± 0.4			6
P305X	0.24 ± 0.04	2.2 ± 0.8			5
L306X	0.19 ± 0.02	2.1 ± 0.5			5
G307X	0.17 ± 0.02	1.6 ± 0.4			5

Supplementary Table 5 | Data statistics for ELIC recordings with voltage clamp fluorometry (VCF)

Current values and corresponding fluorescence changes for concentration-activation curves obtained from fluorescently labelled ELIC cysteine mutants or ANAP labelled mutants. Data are reported as the mean ± SEM from 5 to 7 independent experiments.

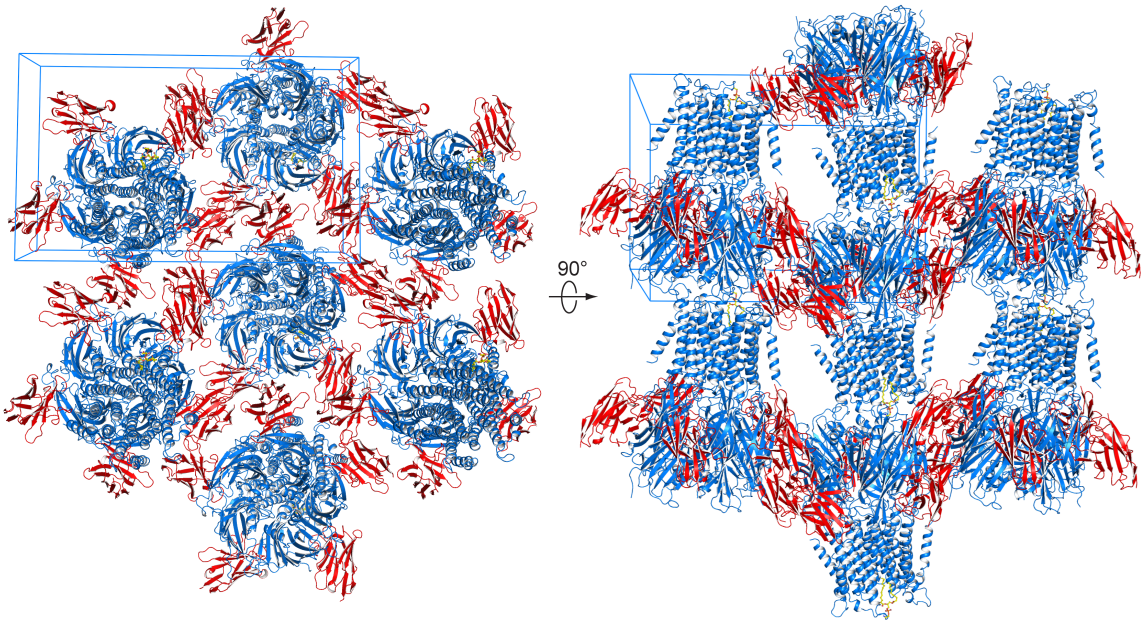

Supplementary Figure 1 | Crystal packing for ELIC 7'C-nanobody 72 structure. The ELIC 7'C-nanobody 72 (Nb72) complex crystallizes in a different crystal packing than apo ELIC (PDB code 2vl0) and improves the crystal diffraction limit to 2.5Å. One Nb72 molecule (red cartoon) is bound to one ELIC 7'C monomer (blue cartoon). This crystal packing is stabilized through nanobody-mediated interactions, either between Nb-Nb (chain G, I, J) or between Nb and extracellular domain of ELIC (chain F and H). Additional crystal contacts are between the top of the extracellular domain of ELIC and the M3-M4 linker of a neighbouring pentamer. The blue bars represent the crystallographic unit cell.

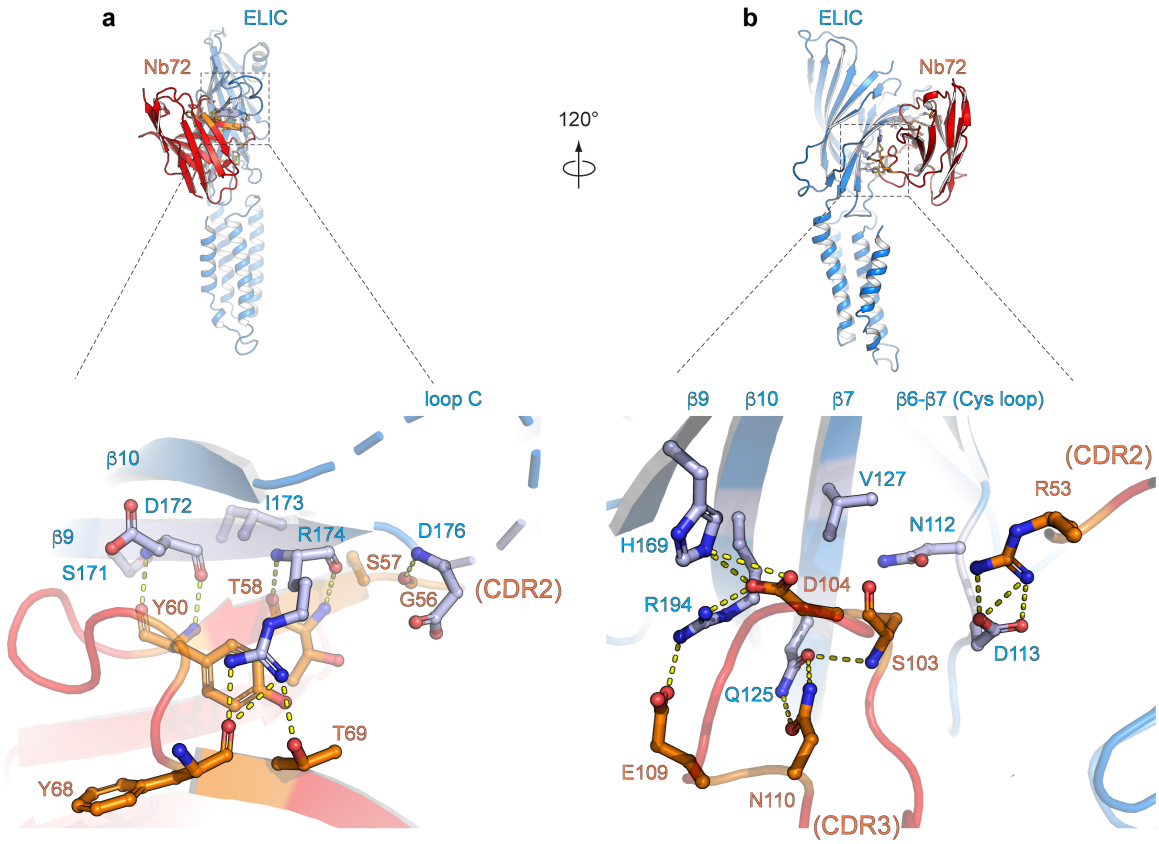

Supplementary Figure 2 | ELIC-Nb72 interaction interface.

Nb72 (red) binds with a unique binding mode to ELIC (blue), which is different from previously reported Nb-bound structures of pLGICs, including the 5-HT3R[1] and the $GABA_AR$ β3/α5 subunit chimera[2]. In the Nb72-bound ELIC structure, the complimentarity determining region CDR2 forms a distinct anti-parallel β-sheet interaction with the β9-strand preceding the tip of loop C in ELIC (**a**). The interactions are mainly formed by main chain atoms, for example hydrogen bonds are formed between the pairs Y60(Nb)-D172(ELIC), T58(Nb)-R174(ELIC) and G56(Nb)-D176(ELIC). The R174(ELIC) side chain forms additional interactions with Y68-T69(Nb) main chain atoms. In contrast, the residues from the CDR3 region are mainly involved in interactions between side chains, for example S103, E109, N110 (Nb) and H169, R194 (ELIC) (**b**).

1. Hassaine, G. *et al.* X-ray structure of the mouse serotonin 5-HT3 receptor. *Nature* **512,** 276–281 (2014).
2. Miller, P. S. *et al.* Structural basis for GABAA receptor potentiation by neurosteroids. *Nat Struct Mol Biol* **24,** 986–992 (2017).

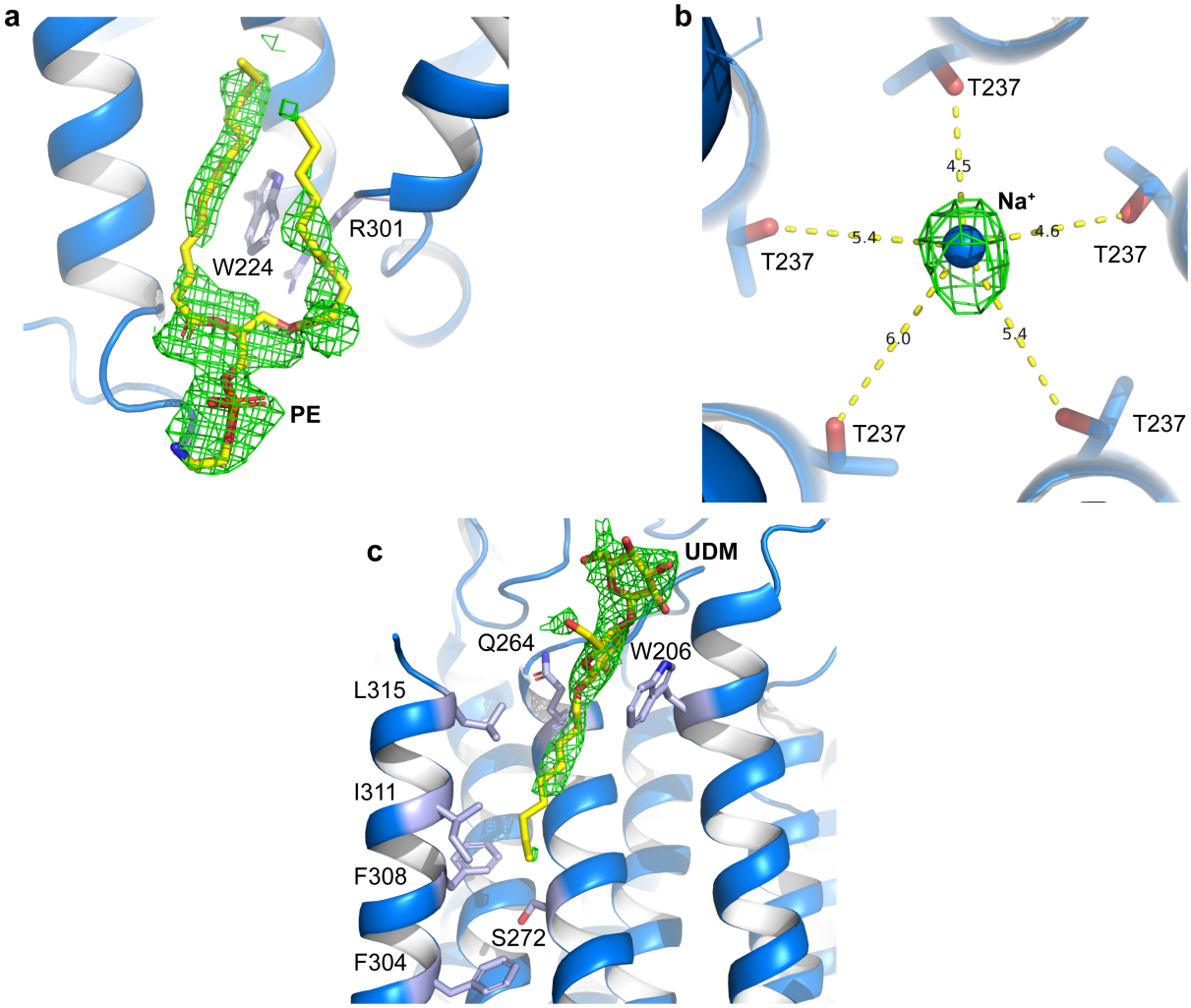

Supplementary Figure 3 | Omit maps for lipid, ion and detergent.

The green mesh shows the electron density calculated from a simulated annealing composite omit map ($2F_o$-F_c) for phosphatidylethanolamine (**a**, PE, contoured at 1σ), a Na^+ ion bound in the channel pore (**b**, T237 corresponds to the 6' pore position, contoured at 1.5σ) and an n-undecyl-β-D-maltoside detergent molecule (**c**, UDM, contoured at 1σ). ELIC is shown in blue cartoon presentation. Surrounding side chains are shown as light blue sticks. Light blue corresponds to carbon, red nitrogen, dark blue oxygen.

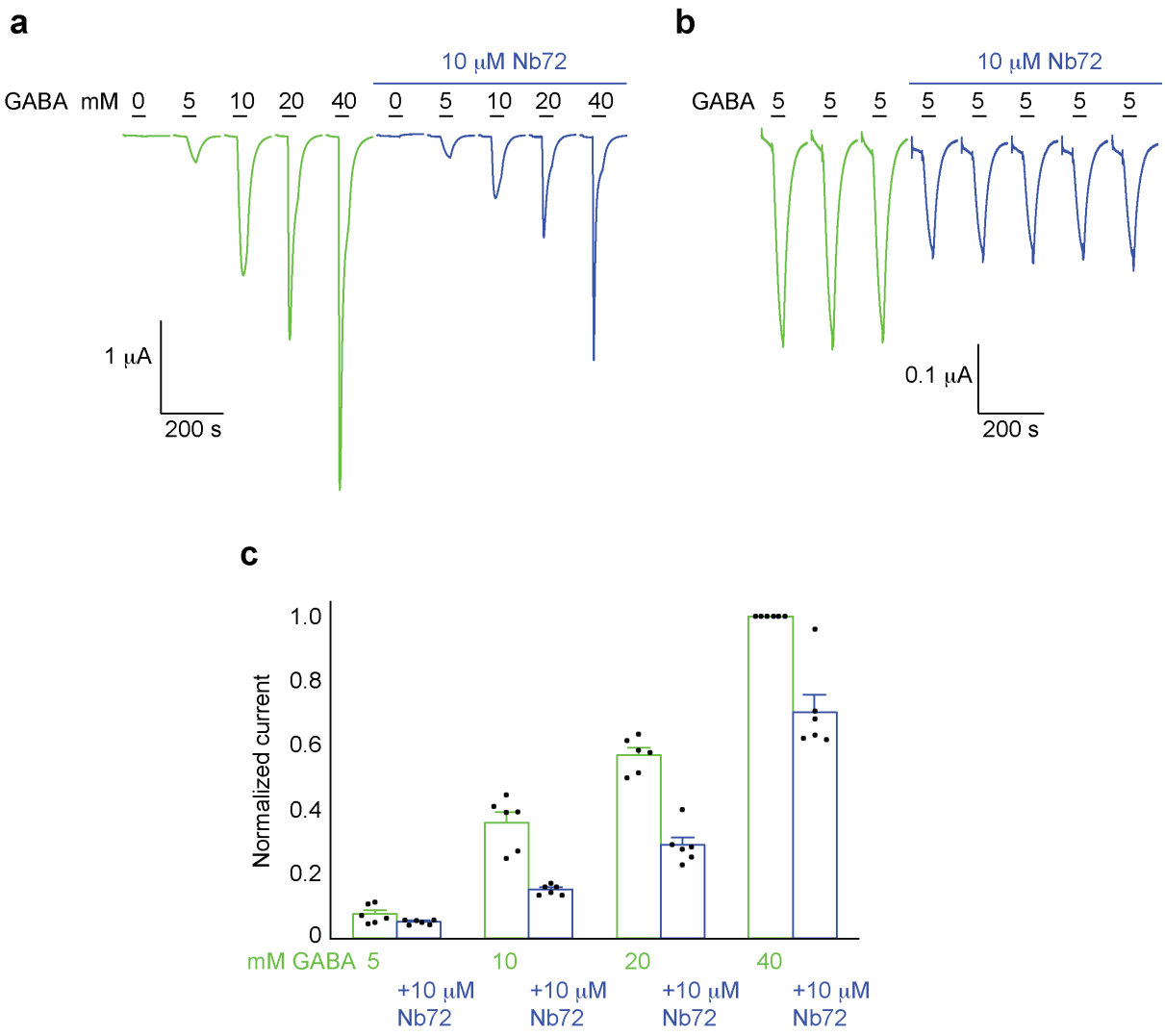

Supplementary Figure 4 | Functional characterization of Nb72 on ELIC.

Functional characterization of the effect of Nb72 on ELIC 7'C channels expressed in *Xenopus* oocytes and using two-electrode voltage clamp recordings. **a**, Agonist responses to 0-5-10-20-40 mM GABA in the absence of Nb72 (green traces) and in the presence of 10 μM Nb72 (blue traces). Representative traces are shown from 6 independent experiments. **b**, Repetitive application of 5 mM GABA, causing little to no channel desensitization, in the absence (green traces) and presence of 10 μM Nb72 (blue traces). Representative traces are shown from 6 independent experiments. **c**, Bar graphs showing averaged current responses ± SEM from experiments shown in (**a**) for n = 6. Data were normalized to the maximal current response with 40 mM GABA in the absence of Nb72. The black dots overlaid with each bar graph represent a dot plot of the individual data points for each set. These results demonstrate that Nb72 reduces the agonist-induced response.

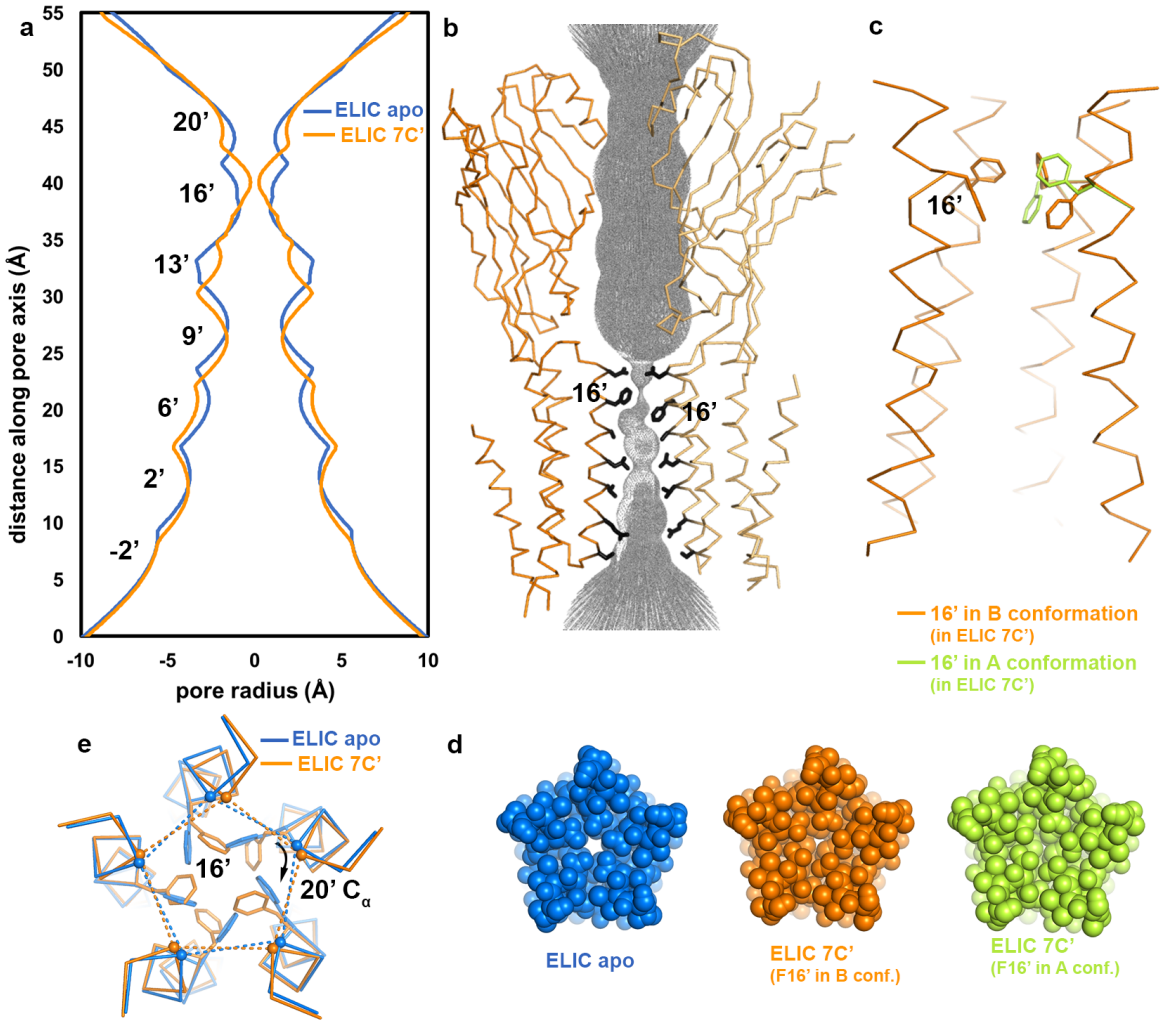

Supplementary Figure 5 | Pore analysis of ELIC 7'C-Nb72 structure.

The pore of ELIC 7'C in complex with Nb72 is slightly more closed than wild type (apo) ELIC (min. pore radii of 0.24 and 0.89 Å, respectively). **a.** The pore profile of the transmembrane domain shows reduced radii for ELIC 7'C (orange) at 13' and 16', as compared with apo ELIC (blue; PDB code 2vl0). **b.** The ion permeation pathway of ELIC 7'C, with 2 subunits shown (Cα-trace; orange and light orange) and the M2 pore-lining residues as sticks (side-chains only; black). The narrowest point in the pathway is at F16'. Pore profiles and ion permeation pathway were generated from the crystal structures using the HOLE program[3]. **c.** The side-view of M2 helices of ELIC 7C' (Cα-trace; orange), with the front subunit removed for clarity. In two of five subunits,

alternative rotamers were observed for F16' (green; at 50 % occupancy). When all subunits are considered there is a "down-up-up-down-up" and an "up-down-up-down-up" combination for F16'. The alternative conformation (green) is slightly more closed than apo ELIC based on HOLE analysis (min. pore radii of 0.34 and 0.89 Å, respectively). **d.** The top-view of the M2 helices, represented as Van der Waals spheres, also shows that apo ELIC (blue) is less closed than ELIC 7'C (for both sets of F16' conformers; orange & green). **e.** The top-view of the M2 helices of ELIC 7C' and apo ELIC superposed using Cα atoms (root mean square difference: 0.48 Å). ELIC 7'C appears twisted compared to apo ELIC, with the 20' Cα atoms (shown as small spheres) rotated for ELIC 7'C compared to apo. This top-view also shows the contrast in the F16' side-chain orientations between the apo and mutant ELIC.

3. Smart, O. S., Neduvelil, J. G., Wang, X., Wallace, B. A. & Sansom, M. S. HOLE: a program for the analysis of the pore dimensions of ion channel structural models. *J Mol Graph* **14,** 354–60–376 (1996).

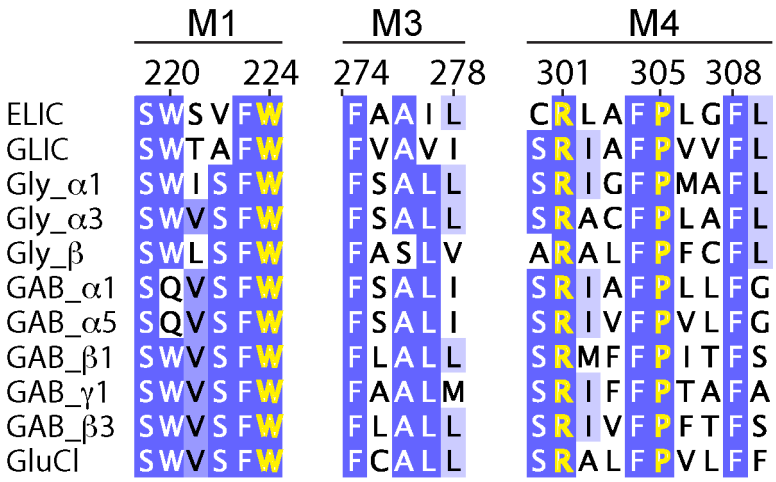

Supplementary Figure 6 | Sequence alignment of residues forming the lipid binding site in ELIC

The sequence alignment shows highly conserved residues of the lipid binding site in ELIC and compared to anion-selective eukaryote pLGICs. “Gly” indicates glycine receptors, “GAB” indicates $GABA_A$ receptors and GluCl indicates the invertebrate glutamate-activated chloride channel. Shades of blue indicate sequence conservation with an identity threshold of 40%. Residues of the W-R-P triad are highlighted in yellow.

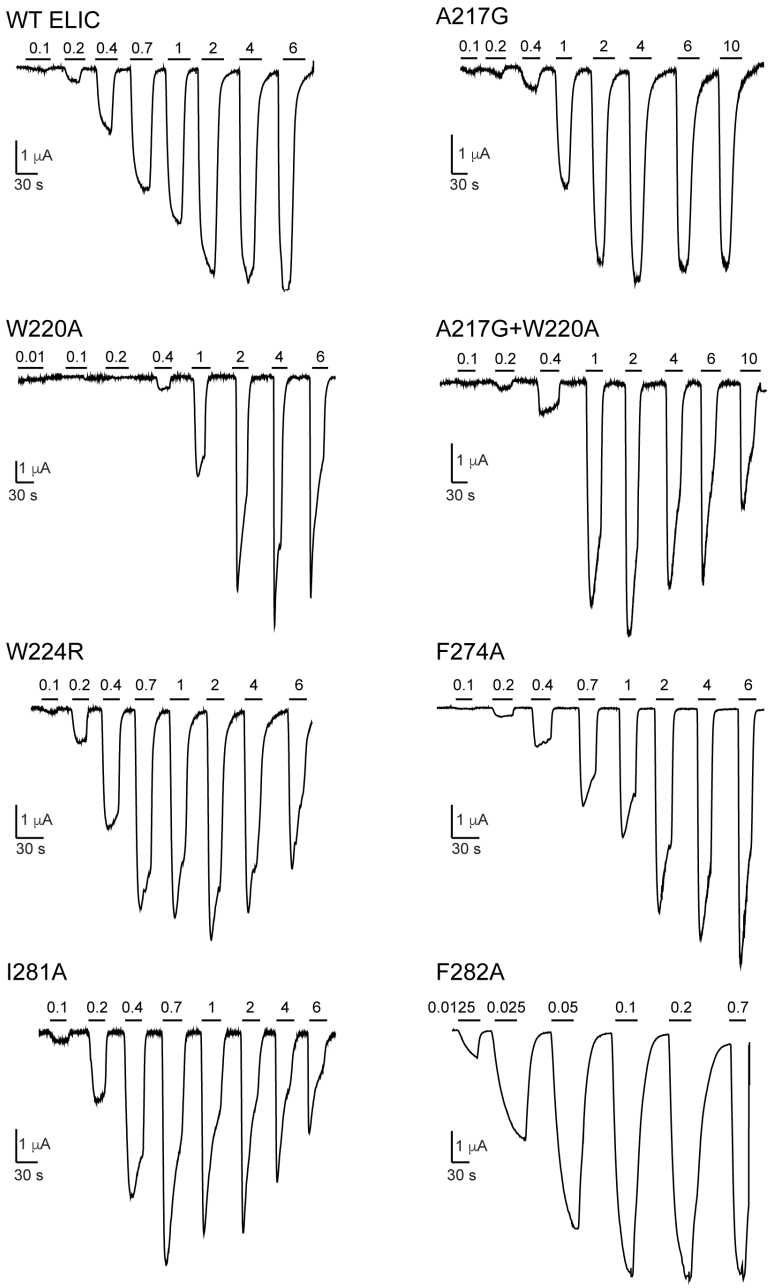

Supplementary Figure 7 | Electrophysiological characterization of ELIC mutants in the lipid binding site.

Functional characterization of single mutants of amino acid residues composing the PE lipid binding site. Mutants were expressed in *Xenopus* oocytes and responses to increasing concentrations of the agonist cysteamine were measured using two-electrode voltage clamp recordings. All identified mutations have relatively minor changes in the EC_{50}-values for cysteamine, except F282A which becomes more 20-fold more sensitive than wild type ELIC. Compared to wild type ELIC, all other mutants display more rapid desensitization kinetics, which is similar but less drastic than the P305A mutant. Representative traces are shown from 3-9 independent experiments

for each construct. Slope values for these mutants are reported in Supplementary Table 3 and were obtained by plotting the reciprocal time constant of activation ($1/\tau$) as a log function of agonist concentration (identical to the procedure used in Supplementary Figure 8).

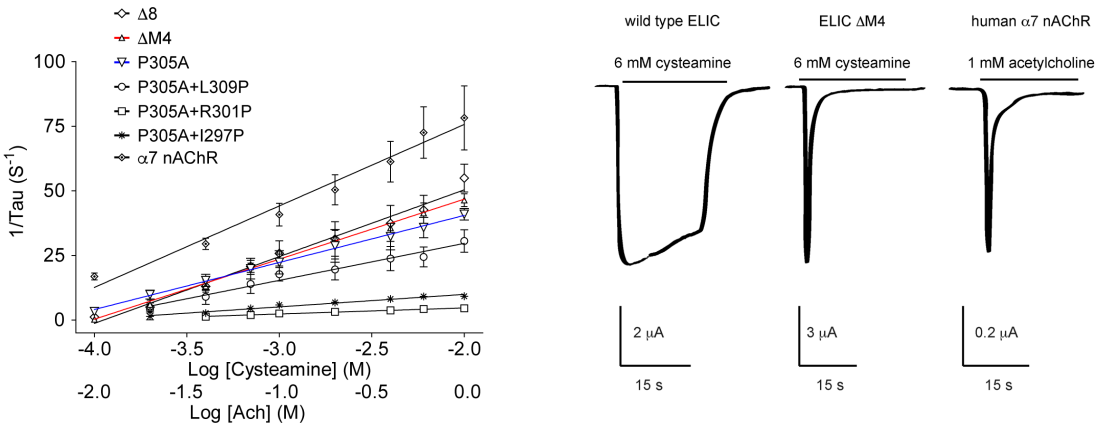

Supplementary Figure 8 | Quantitative analysis of ELIC desensitization kinetics. Analysis of densensitization kinetics for the ELIC current traces shown in Figure 3. This data plot is the reciprocal time constant of activation ($1/\tau$) as a log function of agonist concentration. Cysteamine was used as agonist for ELIC, acetylcholine for the α7 nAChR. Values are presented as the mean ± SEM from 4 to 8 independent experiments. These data were fit with a linear function and the slope values are reported in Supplementary Table 4. Example traces on the right are shown for the slowest desensitizing channel in this study, ELIC, as well one of the fastest desensitizing mutants (ΔM4), which has comparable fast desensitization kinetics to the human α7 nAChR. Representative traces are shown from 4-8 independent experiments for each construct.

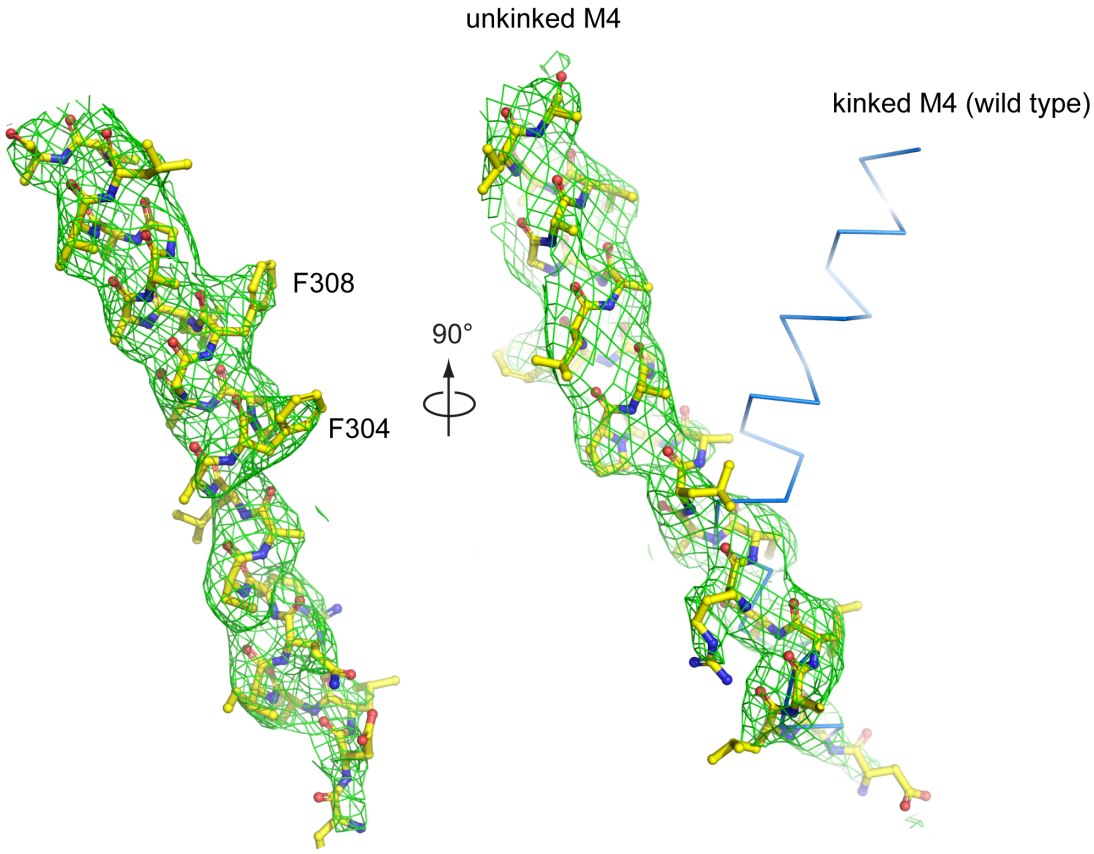

Supplementary figure 9 | Electron density map for the alternate M4 conformation in ELIC.

Electron density map for the alternate conformation of the M4-helix in the 3.45 Å structure of ELIC F16'S. The green mesh shows the electron density calculated from a simulated annealing composite omit map ($2F_o$-F_c) contoured at a level 1σ for the unkinked conformation of the M4 helix in chain J. The stick representation shows M4 residues 293-317 of ELIC F16'S, yellow corresponds to carbon, red oxygen, blue nitrogen (left). The protruding densities for the F304 and F308 residues helped to establish the correct register of the helix in this conformation. For reference, the right panel shows a superposition with wild type ELIC (PDB code 2vl0) shown as a blue ribbon.

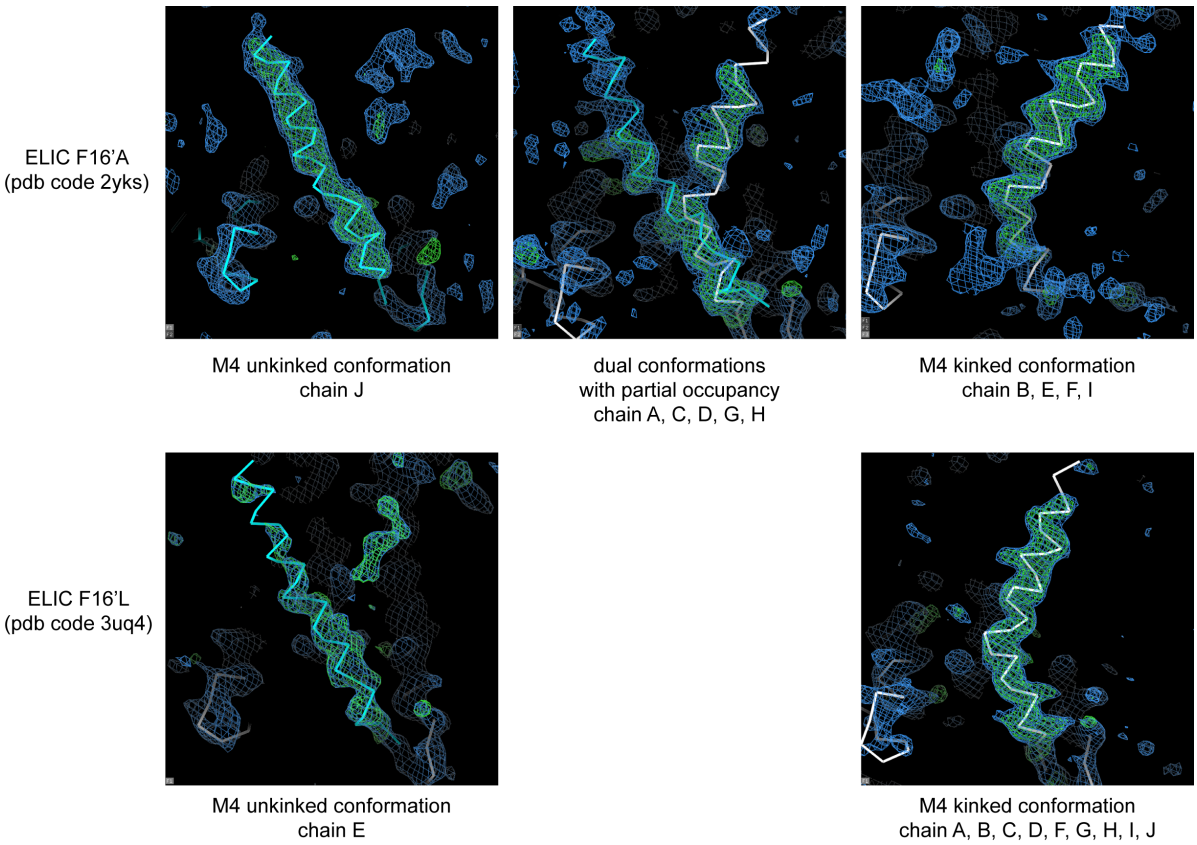

Supplementary Figure 10 | Examples of previously published ELIC structures with electron density indicating the alternate M4 conformation.

A survey of previously published ELIC structures reveals additional examples in which the M4-helix adopts the same alternate conformation as observed in this present study. This is especially true for other structures of the F16' pore mutant, suggesting that this mutation might allosterically stabilize the alternate conformation. Electron density maps are shown for ELIC F16'A with PDB accession code 2yks (ref [4]) and ELIC F16'L with PDB accession code 3uq4 (ref [5]). The blue mesh corresponds to $2F_o$-F_c density contoured at a level of 1σ and the green density corresponds to F_o-F_c density contoured at a level of 3σ. These maps were obtained by deletion of the M4-helix residues and refinement in Refmac with tight non-crystallographic symmetry (NCS) restraints for each monomer. Left are examples of the M4 unkinked conformation, center are dual conformations with partial occupancies, and right the M4 kinked conformation.

4. Zimmermann, I. & Dutzler, R. Ligand activation of the prokaryotic pentameric ligand-gated ion channel ELIC. *PLoS Biol* **9,** e1001101 (2011).
5. Gonzalez-Gutierrez, G. *et al.* Mutations that stabilize the open state of the Erwinia chrisanthemi ligand-gated ion channel fail to change the conformation of the pore domain in crystals. *Proceedings of the National Academy of Sciences* **109,** 6331–6336 (2012).

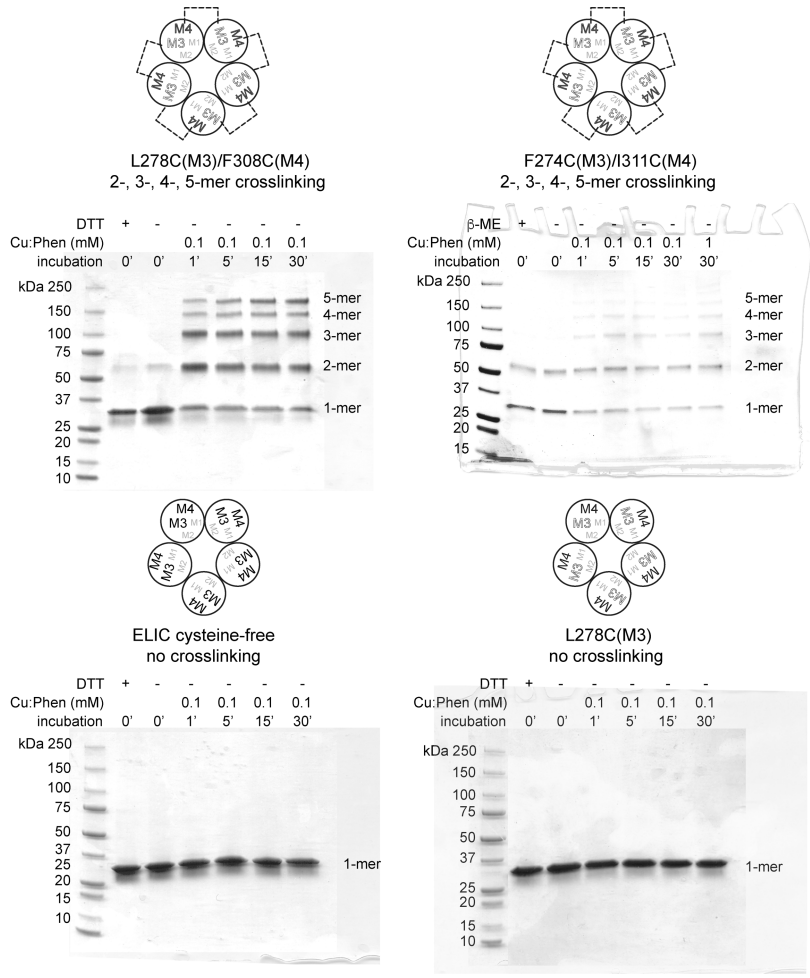

Supplementary Figure 11 | Cysteine crosslinking of double cysteine mutants engineered in ELIC M3/M4

Crosslinking experiments with double cysteine mutants in M3/M4 of detergent-solubilized ELIC. The L278C(M3)/F308C(M4) mutant contains two cysteines, which are in close enough proximity to allow disulphide bond formation in the unkinked M4 conformation. Consistent with this view, we observe band shifts corresponding to the formation of 2-mer, 3-mer, 4-mer and 5-mer crosslinked subunits under oxidizing conditions, indicating that the intersubunit interactions observed in the crystal structure are sampled as part of the M4 dynamic landscape. Similar results are seen for the F274C(M3)/I311C(M4) mutant. No crosslinking is observed in the negative controls, cysteine-free ELIC and L278C(M3) single mutant. Each construct was tested in duplicate with similar results. The uncropped part of the gel scan is presented in lighter shading. These results suggest that in detergent micelles, ELIC adopts the unkinked M4 conformation.